ADVANCED MATERIALS TECHNOLOGIES
www.advmattechnol.de

High-Resolution Scanning Probe Nanolithography of 2D Materials: Novel Nanostructures

*Ekta Rani and Lu Shin Wong**

2D materials have attracted tremendous research interest since the isolation of graphene. Their remarkable optical, electronic, and mechanical properties show that they hold great potential across a range of technological applications. As a result, there is a growing demand for low-cost, low-energy, and high-resolution lithography methods that will enable the integration of 2D materials into complex integrated circuitry, biomedical devices, and in the generation of quantum-confined nanostructures. Recent advances in scanning probe nanolithography (SPL) techniques for the lithography of 2D materials such as graphene, black phosphorus, molybdenum disulfide, and tungsten diselenide are discussed, including the various physiochemical aspects of subtractive and additive lithography of these materials. Examples of 2D-material-based devices fabricated by SPL and their properties are also described. The comparative advantages of the individual SPL techniques are discussed along with the future outlook of SPL for 2D materials.

1. Introduction

Since the isolation of graphene in 2004,[1] interest in 2D materials has progressed rapidly and sparked a whole new field of research. 2D materials are atomically thin layered crystalline solids with no dangling surface bonds, which have intralayer covalent bonding and interlayer van der Waals bonding.[2–4] The number of 2D materials that have been described has been growing since 2004 and include semimetals such as phosphorene; semiconductors, including transition metal dichalcogenides such as molybdenum disulfide (MoS_2) and tungsten diselenide (WSe_2); and insulators such as hexagonal boron nitride.[5–7] 2D materials are flexible and show superior intralayer (vs interlayer) transport of fundamental excitations (charge, heat, spin, and light), and thus exhibit unique optical, chemical, mechanical, and electrical properties compared to their bulk counterparts.[2–7] Due to these properties, 2D materials have been proposed as components of future flexible devices for nanoelectronics, optoelectronics, tissue engineering, and biosensor applications.[2–12]

In order to advance these materials toward practical applications, there is a need for lithographic techniques to produce or modify these materials to user-specified designs, ideally at nanoscale resolution. Various conventional lithographic approaches including electron-beam lithography (EBL), photolithography, nanosphere lithography, and ion beam lithography have been reported for this purpose.[13–18] Among these various approaches, EBL followed by a chemical etching is currently the most widely used technique for the fabrication of 2D material-based devices.[13–16] Indeed, EBL is perhaps the benchmark in terms of nanolithography resolution, precision, and accuracy (down to sub-10 nm).[19] However, it requires ultrahigh vacuum conditions and is a time-consuming serial process, and therefore not amenable to scale-up for industrial mass production. Furthermore, EBL resist coatings leave residues that are difficult to remove completely and negatively impact the materials' properties.[16] The harsh chemical reaction conditions used in conventional etching also results in rough edges with dangling bonds, defects, and the formation of various functional groups can further affect the properties of the materials.[20–22] Similarly, ion beam lithography has also been demonstrated as a useful tool for precisely manipulating graphene.[23,24] However, the feature size and edge definition is limited due to the possible diffusion of ions into the substrate. Photolithography is another commonly used method,[14,17,18] and one which enables large-area lithography. However, it suffers from many of the same drawbacks as EBL such as the requirement of costly equipment, and the use of resist materials can adversely affect the properties of the 2D material.

The limitations of conventional lithography techniques have thus stimulated the development of "unconventional" nanolithographic fabrication methods. In this regard, scanning probe nanolithography (SPL)[25–27] has emerged as a "resist-free," robust and versatile family of lithographic techniques that combine nanoscale spatial accuracy and registry with the ability to directly pattern various soft materials (e.g., small organic molecules, polymers, and biomolecules) under ambient conditions, and in several cases without the requirement of an etching step. Here, SPL uses the tip of a scanning probe microscope to create nanopatterns on the surface by employing a

Dr. E. Rani,[+] Dr. L. S. Wong
Manchester Institute of Biotechnology and School of Chemistry
University of Manchester
131 Princess Street, Manchester M1 7DN, UK
E-mail: l.s.wong@manchester.ac.uk

The ORCID identification number(s) for the author(s) of this article can be found under https://doi.org/10.1002/admt.201900181.

[+]Present address: Department of Physical Sciences, Central University of Punjab, Mansa Rd, Bathinda, Punjab-151001, India

DOI: 10.1002/admt.201900181

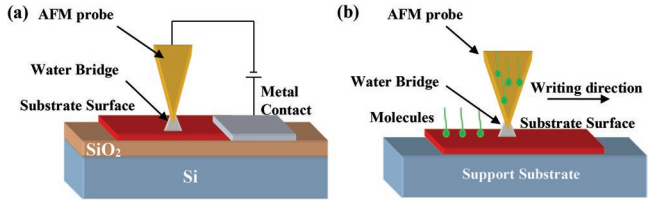

Figure 1. Schematic diagram illustrating a) electrochemical SPL of a substrate deposited on SiO_2/Si, electrically connected by metallic contacts. Under ambient or humid conditions, a water meniscus condenses between the AFM probe and the surface substrate, which acts as the electrolyte for the electrochemical reaction when a bias is applied and b) DPN. In a humid environment, a water meniscus formed between the AFM and the substrate facilitates the transport of molecules to the substrate surface.

variety of physicochemical effects. SPL can be divided into two broad conceptual strategies: "subtractive" or "destructive" SPL involving the removal of material from the surface; and "additive" or "constructive" SPL involving the deposition of material on to the surface.

Subtractive SPL exploits various physical interactions (e.g., electrical potential, heat, applied force) between the probe and the surface to ablate or modify the material(s) already present on the surface. Such subtractive methods include: electrochemical-SPL in which an electrical bias between the probe tip and the surface results in an electrochemical (oxidation or reduction) reaction at the point of contact (**Figure 1**a),[28,29] thermochemical-SPL (tc-SPL) wherein contact of a heated probe with the surface leads to chemical changes,[30–32] and mechanical-SPL (m-SPL) uses mechanical force to scratch the surface as a means of generating nanoscale features.[33]

In additive SPL, the probe is used to deliver molecules in a spatially controlled manner on to the surface. Additive methods include dip pen nanolithography (DPN)[25] and methods derived from it such as polymer pen lithography (PPL).[34] In these methods, the probes are coated with an "ink" formulation and used as a "pen" to "write" the ink on to the surface via a water bridge (Figure 1b). These methods are particularly significant as multiplexed SPL has been demonstrated using parallelized arrays of probes covering cm^2 areas and thus offers scalability.[35]

2. Subtractive ("Destructive") Nanolithography of 2D Materials

2.1. Electrochemical-SPL

Thus far, electrochemical-SPL has been the most widely demonstrated technique for the manipulation of 2D materials. Here, an atomic force microscope (AFM) is used wherein the electrochemical reaction takes place in an in situ generated electrochemical cell consisting of the probe and surface, each acting as an electrode, and the water bridge formed between them acting as an electrolyte (Figure 1a).[36] In general, the main parameters that control the local electrochemical process and resolution of the nanopatterns are the applied voltage across the probe tip and surface (V_{tip}), scanning speed of the tip (v_{tip}), and relative humidity (RH) of the atmosphere around the tip and the surface.

Ekta Rani is currently an assistant professor at the Central University of Punjab, with research interests including soft lithography, spectroscopy, and microscopy for nanofabrication and associated applications. She completed her BSc and MSc degrees at Panjab University in 2008 and 2010, respectively. Subsequently, she joined the Raja Ramanna Centre for Advanced technology to study semiconductor nanocomposites for her PhD with Dr. Alka A. Ingale. In 2016 she joined the Manchester Institute of Biotechnology (MIB), University of Manchester, as a postdoctoral research associate with Dr. Lu Shin Wong and Prof. Royston Goodacre, researching the development of scanning probe lithography-based bio–sensors.

Lu Shin Wong is a lecturer at the School of Chemistry and group leader at the Manchester Institute of Technology (MIB), University of Manchester. He holds a Bachelor of Pharmacy (BPharm, University of Nottingham) and undertook his PhD studies in organic and analytical chemistry with Prof. Mark Bradley (University of Southampton). In 2005, he joined the MIB as a postdoctoral researcher under Prof. Jason Micklefield. In 2008, he received an EPSRC Life Science Interface research fellowship to work with Prof. Chad A. Mirkin (Northwestern University). He returned to his current position at Manchester in 2011, working at the bio–nano interface.

2.1.1. Oxidation of Graphene

The most common variant of electrochemical-SPL is oxidative scanning probe lithography (o-SPL, also previously referred to as "local anodic oxidation"),[28,37] where the probe tip acts as the cathode. In the case of graphene, a V_{tip} of ≈–10 V is typically applied. Due to the close proximity between the probe and surface (typically ≈ 1 nm), this voltage generates an extremely high localized electric field in the order of 10^{10} V m^{-1} that ionizes water molecules leading to the generation of reactive oxygen-containing species (e.g., OH^-, $O_2^{\bullet-}$), which subsequently oxidizes the surface. Since a substantial amount of work has been published on the oxidation of graphene,[38–60] this review will instead focus on a smaller number of selected case studies that relate to the physicochemical aspects of SPL, and the use of SPL for device fabrication.

The first example of o-SPL on graphene was reported in 2008 by Giesbers et al.[38] Here, linear features with a width of ≈30 nm were generated by lithography on single layer and bilayer graphene (SLG and BLG, respectively) substrates using a scanning probe in contact mode with a V_{tip} of −25 V, a v_{tip} of 50 nm s^{-1} and at an RH of 55%. Authors proposed that under these conditions o-SPL leads to the formation of volatile carbon-based oxides in the patterned region that evaporate to leave a trench where the graphene layer(s) have been etched away.

Weng et al.[39] have reported lithography of multilayer graphene (MLG) in tapping mode with a V_{tip} in the range of −15 to −30 V. However, in contrast to the above example, tapping mode[61] AFM measurements postlithography showed raised features at a V_{tip} of −16 V (**Figure 2**a), which the authors proposed were the result of the formation of graphene oxide (GO) that possessed an increased volume due to the incorporation of oxygen. For V_{tip} magnitudes greater than −16 V, trench formation was observed (Figure 2a) that was consistent with the formation of volatile carbon oxides,[62] as noted above. To demonstrate the use of o-SPL to fabricate MLG flakes, the authors showed that a trench written across half of an MLG flake resulted in an increase in the resistance between the two ends of the flake from 6.3 to 7.5 kΩ; while extending the trench through the whole flake (Figure 2b) resulted in the loss of electrical contact (infinite resistance) indicating that it had been completely cut.

Masubuchi et al.[40] have described lithography of SLG, BLG, and MLG in tapping mode with a V_{tip} of −35 V at RH in the range of 39% to 44% and a v_{tip} ranging from 10 to 160 nm s^{-1}. Under these conditions it was instead observed that the lithography resulted in trenches with raised features on either side (Figure 2c–e). Postlithography resistance measurements performed across a raised feature gave a large resistance (>1 GΩ), which authors thus proposed were GO. Subsequent lithography

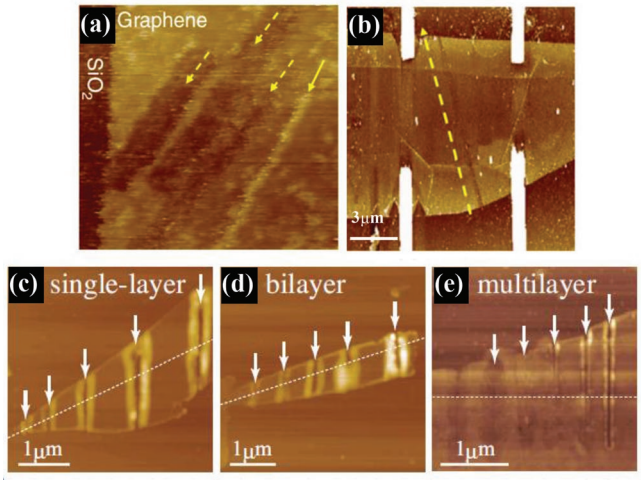

Figure 2. AFM topography images of graphene substrates post o-SPL showing a) three trenches (marked with dashed arrows) and one raised feature (marked with solid arrow), b) a trench cut through the entire flake. The four white bars in (b) are the metal contacts fabricated using EBL. AFM topography images of c) single layer, d) bilayer, and e) multilayer graphene after the lithography was carried out in the direction indicated by the white arrows at the v_{tip} of 160, 80, 40, 20, and 10 nm s^{-1} (left to right). Reproduced with permission.[40] Copyright 2009, AIP Publishing.

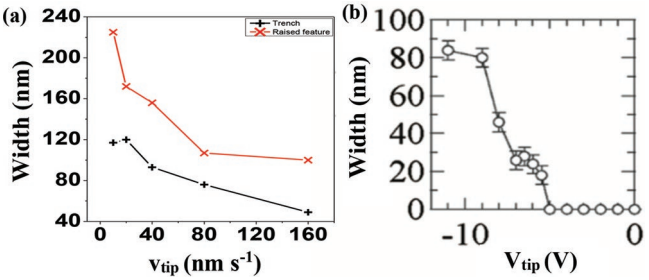

Figure 3. a) Graph of the width of the trench and raised feature against v_{tip} for SLG and b) width of the oxidized region against the lithography V_{tip} (at a v_{tip} of 50 nm s^{-1}). b) Reproduced with permission.[42] Copyright 2011, American Chemical Society.

performed with various v_{tip} showed that lower speeds resulted in wider trenches and raised features, although the relationship between the v_{tip} and width of trench/raised features is found to be nonlinear (on SLG, **Figure 3**a).

In a follow-on study,[42] Masubuchi employed o-SPL in contact mode on SLG with a lower V_{tip} in the range of 0 to −9 V to investigate the threshold voltage (V_{thresh}) required for the formation of GO (at 75% RH, v_{tip} of 50 nm s^{-1}). It was found that no features were observed until a V_{tip} of −5.5 V was applied, at which point raised features ≈20 nm in width were observed. An increase in the magnitude of V_{tip} to −9 V led to an increase in the width to 50 nm (Figure 3b). Subsequent Raman spectroscopy of these features gave spectra comparable to those observed in chemically produced GO.[63] Based on these observations, authors concluded that o-SPL at this lower voltage range leads to the formation of GO features. A parallel report by Park and co-workers[44] on the o-SPL of SLG and BLG followed by Raman analysis also came to the similar conclusions, but they additionally studied the effect of V_{tip} and v_{tip} (at 20% RH) on the width of the GO line features on SLG. At a fixed v_{tip} of 100 nm s^{-1}, the V_{thresh} was found to be −5 V and led to the formation of ≈45 nm wide lines, while −7 V gave features of 55 nm. Conversely, the line width was found to be 82 and 61 nm for v_{tip} of 100 and 1000 nm s^{-1}, respectively at a V_{tip} of −10 V.

A comparative analysis of SLG o-SPL described by Masubuchi[42] and Park[44] shows that narrower lines are formed at a higher RH and lower v_{tip}. This observation is notable since a lower RH and higher v_{tip} would have been expected to give narrower features because of a smaller volume of the water meniscus and shorter interaction time. However, Masubuchi et al.[42] employed lower contact force (<1 nN), whereas Park and co-workers[44] employed a contact force of 1 nN. Thus, the observed differences could be due to the difference in the contact force used during the lithography.

o-SPL of graphene has also been studied using micro-X-ray photoelectron spectroscopy (μ-XPS),[50] whereby lithography was performed with V_{tip} in the range of −5 to −10 V at an RH of 30%. For graphene oxidized at −5 V, two peaks in the carbon region of the XPS spectrum corresponding to sp^2 C—C and C—OH functional groups were observed. At −7 and −10 V, the spectrum showed a reduction in the intensity of the C—C peak and the emergence of peaks corresponding to C—O—C and C=O species. However, it was found that the oxidation of

graphene (ratio of area under the peaks corresponding to C—O/C=O vs C—C bonds) at a V_{tip} of −10 V was similar (≈90%) for SLG, BLG, and three-layer graphene (TLG). This result suggests that all layers were equally oxidized regardless of the thickness of the graphene, and the degree of oxidation was higher than graphene oxidized by the conventional solution-phase Hummers method (79.0%).[64]

In a similar study[60] (with approximately the same V_{tip} and RH), but when graphene with non-Bernal stacking of the layers was used, it was found that the μ-XPS intensity of the peaks corresponding to oxide functional groups increased by tenfold compared to unpatterned graphene, but did not change between SLG, BLG, and TLG. This result suggested that the amount of oxygen incorporated in the BLG and TLG was no different compared to SLG, since oxygen incorporation uniformly across all layers would result in increasing C—O/C=O signal (but constant C—O/C=O to C—C ratio, as noted with the Bernal stacked material noted above). Authors proposed that the most plausible reason for the limited oxygen incorporation was due to the negligible electronic interactions between the layers of the non-Bernal stacked graphene, which therefore resulted in only the topmost layer being oxidized.

Overall, for o-SPL on graphene, these reports suggest that V_{tip} with magnitudes greater than −16 V leads to ablation of the graphene and the formation of trenches. At smaller V_{tip} GO is instead produced, though there exists a critical V_{thresh} ≈−5 V below which no oxidation occurs. Increasing the magnitude of V_{tip} from −5 to −10 V leads to an increase in the width of GO features for a fixed RH and ν_{tip}. Further, at fixed V_{tip}, increase in ν_{tip} leads to a decrease in the width of line features. The structure of GO features formed are also dependent on the type of graphene material, with non-Bernal stacked graphene giving rise to preferential oxidation on the topmost layer.

2.1.2. Reduction of Graphene and Graphene Oxide

Park and co-workers[44] have also employed reductive SPL (r-SPL) to demonstrate reduction (in contrast to oxidation in o-SPL) by the hydrogenation of SLG and BLG. Raman spectroscopic analysis of the features produced with a positive bias (V_{tip} of +7 V) showed the presence of a Raman mode ≈1116 cm^{-1} corresponding to C—H bonds along with G, D, and 2D peaks. Here, the authors proposed that the application of positive V_{tip} led to the electrolysis of water and the formation of reactive hydrogen atoms (H•) on the graphene surface that is acting as the cathode, which in turn led to the hydrogenation. On SLG, it was found that at an RH of 33% and a ν_{tip} of 100 nm s^{-1}, a V_{tip} of +6 V (the V_{thresh}) or +10 V gave line features with a width of 107 or 125 nm, respectively. No significant change in the width (110 nm) was found for various ν_{tip} in the range of 100 to 1000 nm s^{-1} at a V_{tip} of +7 V.

SPL-induced hydrogenations have also been studied with μ-XPS.[50] Here, hydrogen coverage on SLG (as determined by the intensity of peak the corresponding to the C—H group divided by intensity of sp^2 C—C peak) was estimated to be 32.2%, 40.1%, and 49% at V_{tip} of +6, +10, and +20 V, respectively (at 100 nm s^{-1} ν_{tip} and 30% RH), which is higher than that observed for graphene hydrogenated using H_2 plasma (16.6%).[65]

r-SPL has also been used to reduce GO to create patterns of reduced GO (rGO).[66–69] Faucett and Mativetsky[67] have reported the use of SPL to pattern electrically conductive spots of rGO on single layer, bilayer, and multilayer GO (SLGO, BLGO, and MLGO, respectively). It was found that a V_{thresh} of +2.5 V was required to generate features on SLGO (at 1000 nm s^{-1} ν_{tip} and ambient humidity). Conductive AFM (c-AFM) measurements on patterned BLGO subsequently displayed a threefold increase in current through the rGO feature compared to the surrounding GO, and spot features with a full width at half maximum (FWHM) of 4 nm could be produced. Notably, under the same lithography conditions, the FWHM of the rGO spot increased to 40 nm for MLGO, which the authors suggested was due to the shorter tip–Au substrate distance in BLGO that curtailed the lateral spread of the electric field between the tip and GO leading to smaller rGO spot sizes.

Further, the effect of RH on the r-SPL of MLGO was investigated and an increase in FWHM from 19 to 120 nm of the rGO spot was observed with increasing RH from <20 to 80%. In investigating the effect of material thickness on the rate of reduction at an RH of 40%, it was also found that the conductivity of the features on SLGO reached the maximum value after 1 s, whereas, in MLGO the current maximum was reached only after 10 s suggesting that film thickness is an important parameter in the reduction kinetics. Authors proposed that the observed effect was due to weakening electric field strength between the probe and substrate with increasing distance, leading to slower diffusion of H^+ ions into the deeper layers of MLGO.

In general, r-SPL can be used for the local hydrogenation of graphene to give features of increased resistivity, or the reduction of GO to give features of increased conductivity. For the hydrogenation of graphene, a V_{thresh} of +6 V is needed. On the other hand, the reduction of GO to rGO occurs at a V_{thresh} of +2.5 V and increasing V_{tip} leads to an increase in feature size and conductivity of the resulting rGO features, while increasing RH gives rise to larger features due to an increase in the area of the water meniscus. In comparing the r-SPL of graphene and graphene oxide, it appears that a smaller V_{tip} (+2.5 V) is required to initiate the reduction of graphene oxide at similar RH. However, it is difficult to be definitive as one of the reports[67] did not give the ν_{tip}, which may have an effect on the observed results.

2.1.3. Fabrication of Graphene-Based Devices by Electrochemical-SPL

SPL has been used to fabricate graphene-based devices and the first example of this approach was demonstrated through the fabrication of a field effect transistor (FET). In this regard, FETs employing graphene channels have been proposed because of this material's high carrier mobility (≈15 000 cm^2 V^{-1} s^{-1} at room temperature).[70] However, devices fabricated using purely graphene channels are not suitable for logic applications because graphene has no energy gap between the valence and conduction bands. One strategy to open a bandgap in graphene (i.e., to convert it into a semiconductor) is to perform a partial oxidation of the material.

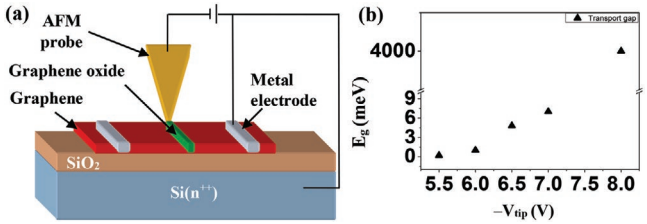

Figure 4. a) Schematic diagram illustrating o-SPL of a single layer graphene on $SiO_2/Si(n^{++})$ giving rise to linear features of graphene oxide and, b) a graph of transport gap energy (E_g) against lithography V_{tip}.

Masubuchi et al.[42] were the first to have demonstrated the use of o-SPL to generate GO features within a graphene channel of an FET. In their experimental setup (**Figure 4**a), two terminal metal electrodes were fabricated on SLG by EBL, and o-SPL was then performed on the exposed SLG with V_{tip} between –5.5 and –9 V (v_{tip} of 100 nm s^{-1}), leading to the generation of GO lines from 20 to 50 nm in width (Figure 3b). In order to test the performance of these FETs, the voltage between the drain and the source electrodes (V_{ds}) and the resulting current was measured as a function of an applied bias on the underlying Si substrate that acted as the gate (V_g). The pristine graphene exhibits a typical V-shaped ambipolar field effect in its bandgap structure, with a minimum conductance (G_{min}) achieved near a V_g of 0 V. Postlithography, conductance measurements of the fabricated device showed systematic decreases in G_{min} from 136 to 0.3 µS with increasing GO line width. The transport gap (E_g) showed an increase from 0.2 to 7 meV as the V_{tip} was varied from –5.5 to –7 V in line with increasing line width (Figure 4b). In the second series of experiments, by maintaining the V_{tip} at –8 V and varying the v_{tip} between 5 to 200 nm s^{-1}, GO line widths of 115 to 48 nm were produced. However, in this case the G was completely suppressed to near zero across the entire V_g range and the E_g (4 eV) was found to be independent of width of the GO lines.

The authors proposed that in the case of moderately oxidized GO, the transport gap of GO (0.2 to 7 meV) is relatively small and the conductance of the device is regulated by localized states in GO. In the case of strongly oxidized GO (achieved with the higher V_{tip} of –8 V) where the energy gap is sufficiently large (4 eV), formation of Schottky barriers at the graphene/GO interface was proposed. This first example of engineering graphene-based FETs using o-SPL thus demonstrates how the properties of the FET can be controlled by the lithography parameters.

Apart from purely graphene-based FETs, SPL has also been applied to devices consisting of heterostructured materials. Levy and co-workers[71] have employed SPL to engineer the electron transport in an FET consisting of a $LaAlO_3/SrTiO_3$ heterostructure with a graphene top gate. The $LaAlO_3/SrTiO_3$ interface is of interest as it exhibits a sharp insulator to conductor transition when the $LaAlO_3$ layer thickness is ≥4 unit cells of this material.[72] Just below this thickness, the interface is insulating but can be reversibly switched, either by local electrochemical-SPL, or by a bias applied through a top gate electrode. For the device fabrication, a positively biased tip (V_{tip} ≈ +10 V: r-SPL) scanned in the contact mode at a v_{tip} of 1000 nm s^{-1} can be used to produce a conducting "nanowire" channel (width ≈ 10 nm) at the $LaAlO_3/SrTiO_3$ interface, which passes under the graphene gate (**Figure 5**a). The nanowire segment directly underneath the graphene thus serves as the active region of the device, where electrons accumulate locally at the interface during the lithography process. It was found that application of V_g led to a steady increase in the conductance (source to drain) with an abrupt increase in the conductance at 6 V indicating the metallic transition of oxide interface. This transition was reversible and thus represented robust FET gating behavior. This report therefore demonstrates the ability to create $LaAlO_3/SrTiO_3$ conducting nanostructures "under" the graphene, which would not be possible if a conventional metal top gate was used.

o-SPL on SLG has also been used to create devices with a FET design that can act as nonvolatile memory.[53] Here, an SLG flake with a 72 nm FWHM GO line written by o-SPL (at a V_{tip} of –9 V, RH of 35%) showed an abrupt lowering in resistance with V_{ds} values >3 V. The device maintained this low resistance state subsequently even when a minimal bias was applied, demonstrating this state was stable. Furthermore, when the V_{ds} was increased to ≈11 V, the device was able to switch back to its original high-resistance state and also maintained this state subsequently. This switching between the two states could be performed repeatedly, demonstrating an example of nonvolatile memory.

The use of o-SPL to fabricate graphene capacitors has also been reported by Seo and co-workers[45] based on SLG on a Si substrate with a thick (300 nm) oxide layer (Figure 5b). Lithography with the V_{tip} applied as a square wave of –8 to –40 V at a frequency of 100 Hz, and a v_{tip} of 400 nm s^{-1} was used to create trenches on graphene and produce isolated "cells" of varying size (Figure 5c). This V_{tip} was much higher than that when graphene layer was grounded directly as mentioned in

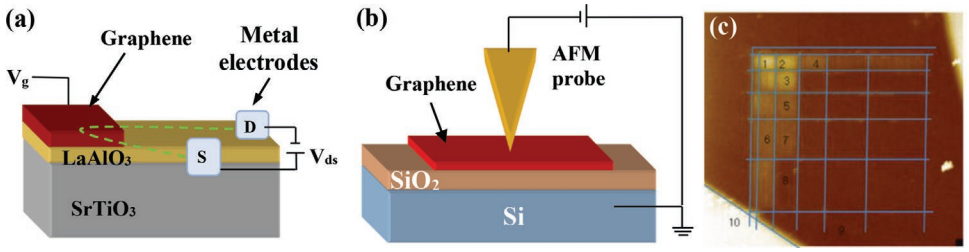

Figure 5. Schematic diagram illustrating a) a top gated graphene and two interface-connected metal source (S) and drain (D) electrodes, the conducting channel fabricated using SPL is indicated by the dotted green line and b) o-SPL of graphene used to fabricate a graphene-based capacitor. c) An EFM image of the substrate postlithography showing charge storage in cells with a range of sizes. (c) Reproduced with permission.[45] Copyright 2012, Elsevier.

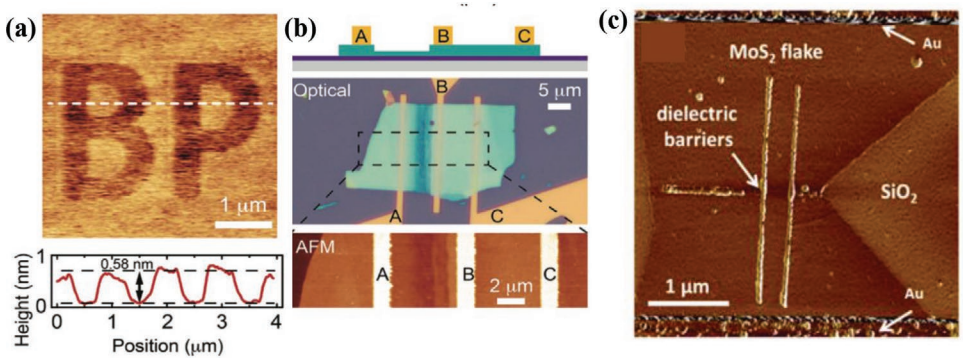

Figure 6. a) AFM topography image of monolayer patterning on BP, with a cross-section corresponding to the dashed line on the image; b) schematic, optical microscopy image, and AFM topography image of BP FETs fabricated with AC patterning (between electrodes A and B) and pristine BP (between electrodes B and C) on 300 nm Si/SiO_2. c) AFM phase image shows the "dielectric barriers" labeled in the figure are MoO_3 lines written by o-SPL on MoS_2, and the "Au" are the source and drain contacts. (a,b) Reproduced with permission.[73] Copyright 2009, John Wiley and Sons. (c) Reproduced with permission.[78] Copyright 2015, AIP Publishing.

the reports above, due to the need to produce sufficient current to initiate the oxidation through the SiO_2 layer. Subsequent electrostatic force microscopy (EFM) imaging measured with a tip bias of 2 V showed a contrast between the graphene outside the patterned areas and the closed cells, showing that each cell was insulated from the bulk surface by the trenches produced through o-SPL. Time dependent EFM measurements also showed that the smaller cells were able to retain a charge for up to ≈70 min, thus demonstrating charge storage.

These reports, therefore, show that o-SPL can provide an alternative and readily accessible method for producing a variety of electronic devices on graphene. By varying the lithography parameters, it is possible to engineer/tune device characteristics, because it is possible to controllably alter the conductivity of the graphene component by altering the degree of "doping" with oxygen through SPL.

2.1.4. Electrochemical-SPL of Other 2D Materials

SPL on Black Phosphorous (Phosphorene): To date, there is only one report of o-SPL on black phosphorous (BP), wherein the lithography was performed on conducting and nonconducting substrates to demonstrate patterning and thinning of BP.[73] On conducting substrates (n-doped Si), a DC bias was used to demonstrate the lithography of arbitrary patterns with resolutions down to ≈50 nm. For RH of between 20% and 50% and at a v_{tip} of 7.5 μm s^{-1}, two regimes were reported: an increase in the magnitude of the V_{tip} from −1.3 to −2.0 V was found to produce features with heights from 4 to 80 nm; while V_{tip} from 0 to −1.2 V produced features from 0 to 6 nm when imaged by tapping mode AFM. However, these same features were observed as depressions by contact mode AFM. The authors explained that since imaging in tapping mode can track the interface of soft materials and fluids, the observed differences indicate the formation of a liquid-like layer in the patterned regions. Subsequent secondary ion mass spectrometry imaging identified O, PO_2, and PO_3 chemical species in these features; and it was also found that these oxides could be removed by washing with water postlithography. These observations suggest the oxidation of the phosphorous to oxoacids that are hygroscopic. Further, authors showed the removal of a single layer of BP when SPL was performed at a V_{tip} of −0.8 V, as attested by the 0.58 nm feature depth (by contact mode AFM, **Figure 6**a). This use of o-SPL for thinning of BP flakes is significant since conventional solution processing[74,75] is incapable of giving such precise control over flake thickness and feature size.

This report also showed the patterning and thinning of BP flakes on a nonconducting substrate (Si substrate with a 300 nm SiO_2 layer) using an AC bias. Here, the AC voltage amplitude was varied between 1.6 and 2.2 V at a frequency of 1 MHz and the etching depth was found to increases with the increase in the amplitude from ≈15 to 31 nm. AC patterning performed at different frequencies from 0.1 to 1 MHz (at 1.8 V and an 8 s dwell time) also revealed that increased oxidation at higher frequencies, as the etching depth was found to increase from ≈10 to 31 nm. Here, the authors of that report proposed that the capacitive charging of the BP allows electron flow to and from the probe as the current alternates, which allows an electrochemical reaction to proceed. This aspect is particularly significant as it demonstrates the possibility of using electrochemical-SPL for nonconducting substrates and thus enhance the application of SPL for patterning and thinning of 2D materials on a wide range of substrates.

For the fabrication of a BP-based device (Figure 6b) on a nonconducting substrate (SiO_2/Si) with AC patterning, a 17 nm thick flake was patterned to produce a linear feature of ≈5 μm and a depth of 9 nm. This flake could then be used as the basis of an FET when connected with source and drain electrodes and the underlying substrate (SiO_2/Si) acting as the gate. Such an FET was found to exhibit a hole mobility of 113 cm^2 V^{-1} s^{-1}, and an on/off current ratio of 10^4 (at a V_{ds} of 2 V). By contrast, an FET produced from a pristine (17 nm thick) flake only gave a mobility of 96 cm^2 V^{-1} s^{-1} and an on/off current ratio of 200; showing that the fabricated device gave superior performance.

SPL on Molybdenum Disulfide: In the case of MoS_2, o-SPL has been shown to generate MoO_3 oxides on five-layered and bulk MoS_2 with resolutions down to ≈2 μm.[76] Here, lithography was performed with a V_{tip} between −3 and −9 V, an RH of 50% and probe dwell times of 0.5 to 2 s on each spot

feature. Notably, an analysis by XPS found that the last layer of MoS_2 could not be oxidized even with 2 s dwell time at −9 V. The authors suggested this effect was due to the presence of the underlying Au conducting layer, though it is unclear how its presence retards the oxidation reaction. The MoO_3 is water soluble and thus can be readily removed leaving the monolayer MoS_2. The authors also showed that MoS_2–MoO_3 heterostructures showed enhanced photoluminescence intensity compared to pristine monolayer and multilayer MoS_2, suggesting that o-SPL may be a useful method for the engineering of heterostructure properties.

Donarelli et al.[77] have described electrochemical-SPL of multilayer MoS_2 with the application of V_{tip} between −6 and −12 V, a 50% RH and a 100 nm s^{-1} v_{tip}, producing patterned spots of ≈550 nm in diameter. However, in this report XPS analysis indicated desulfurization (i.e., removal of sulfur) but no concomitant oxidation to MoO_3, which the authors speculated was due to sulfur desorption induced by OH^- ion "bombardment" of the molybdenite surface. This report is notable as it demonstrates that, even with a lithography setup which is similar to o-SPL, an entirely different chemical outcome can result. It therefore suggests that there are experimental factors that are currently unaccounted for (and remain poorly understood) in the lithography literature.

In terms of device fabrication, Garcia and co-workers[78] have demonstrated the use of o-SPL to fabricate MoS_2 monolayer-based FETs. For this purpose, MoO_3 lines ≈200 nm wide were written to reduce the electron path between the source and drain electrodes with a voltage pulse amplitude of −54 V at 45% RH (Figure 6c). Notably, the authors comment that enriching the local environment with ozone apparently facilitated the lithography. However, no further details were provided in this aspect. In terms of device performance, the current ratio between the FET fabricated using pristine MoS_2 and the patterned MoS_2 was found to be 12.4 (at a V_g and V_{ds} of 20 and 0.05 V, respectively), which the authors concluded were consistent with the constriction of the channel from 2100 to 200 nm after lithography.

SPL on Tungsten Diselenide: Most recently, o-SPL has been reported on mechanically exfoliated multilayered WSe_2 flakes with thicknesses ranging from 4 to 12 nm.[79] Here, a V_{tip} between −9 and −29 V, an RH of 50%, and probe dwell times of 0.2 to 2 ms were tested in order to generate dot features. It was found that dot features with an FWHM from 28 to 43 nm and heights ranging from 2 to 8 nm were observed (by AFM) at a V_{tip} between −9 and −15 V and probe dwell times of 0.3 to 1.5 ms. The patterned features were found to be readily etched with water, and were thus proposed to consist of WO_3 by the report's authors.

The same report also subsequently described the use of o-SPL to fabricate a WSe_2-based FET. To this end, photolithography was used to pattern the source and drain electrodes at the opposite sides of the WSe_2 flake by electron beam evaporation, with the underlying SiO_2/Si substrate acting as the gate. WSe_2 layers were then treated with oxygen plasma (30 s) to remove any resist residues. o-SPL was then performed to pattern two lines perpendicular to the channel of the FET, to reduce the electron path in a similar manner to the MoS_2 FET discussed above. Etching of the patterned region with deionized water led to formation of a WSe_2 channel with a width of 240 nm. In order to improve the metal/flake contact and the overall electrical performance, the authors also subjected the device to thermal annealing (250 °C for 1 h). It was found that in comparison with an unpatterned WSe_2 channel (width of the channel ≈ 1.3 µm) that had a subthreshold swing (i.e., the gate voltage required to change the drain current by one order of magnitude) of 8.2 V dec^{-1}, the o-SPL patterned device showed a swing and 2.7 V dec^{-1}; indicating superior on-off FET performance.

In further work,[80] the same authors studied the effect of oxygen plasma treatment of WSe_2 on the subsequent o-SPL of this material. When a 15-layer WSe_2 flake that had a native oxide layer was subjected to o-SPL at a V_{tip} of between −12 and −30 V at 35–50% RH and probe dwell times of 0.3 to 9.6 ms the formation of raised dots centered within triangular features was observed. The size of these features increased with increasing dwell time from 0.6 to 1.8 ms for fixed V_{tip} of −16.2 V and 42% RH 42% (**Figure 7**). The authors proposed that the dot feature represented the formation of a large volume of oxide due to multilayer oxidation at the point of contact between the probe and substrate, whereas the triangular component resulted from the formation of a thinner layer of oxides whose growth is self-limited along zig-zag edge orientation of the WSe_2 lattice.

On the other hand, o-SPL performed on oxygen plasma-treated WSe_2 flakes showed isotropic (circular) dot features under similar SPL parameters. Analysis of the patterned surface by Auger electron spectroscopy and AFM indicated that plasma treatment resulted in the formation of a 1 nm oxide layer. Subsequent o-SPL on this oxide layer then gave rise to features consisting of a mixture of W and Se oxides. For example, a dot with a height of ≈1 nm above the surface was produced at a V_{tip} of −24 V, 45% RH and probe dwell times of 2.5 ms. The authors suggested that this oxide layer protected the underlying WSe_2 lattice from the lateral oxidation that was observed in the native oxide-coated WSe_2 surfaces. These results are thus consistent with the earlier paper reviewed above,[79] where triangular features were not observed during device fabrication since oxygen plasma treatment was applied prior to o-SPL.

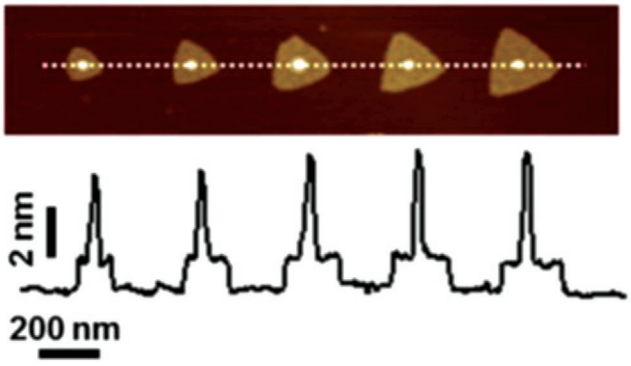

Figure 7. AFM topographic image of patterns fabricated at an RH of 42%, V_{tip} of −16.2 V and probe dwell times of 0.6, 0.9, 1.2, 1.5, and 1.8 ms (from left to right). The cross-section corresponding to the white dashed line is shown. Reproduced with permission.[80] Copyright 2018, American Chemical Society.

Overall, these reports represent proof-of-principle examples of electrochemical-SPL on other 2D materials. In examples of BP, MoS_2, and WSe_2, the reaction products can be removed using water thus demonstrating how a combination of o-SPL and wet etching can be used to produce channels in these materials. The removal of layers of material in this manner gives more precise control of layer thickness (by the adjustment of V_{tip}) compared to conventional exfoliation or solution processing. Nevertheless, in many cases detailed studies of the products of SPL are still required to better understand the observed physicochemical changes. It is clear that several distinct chemical processes have been observed in different reports, even though similar parameters of SPL were used. The results from the WSe_2 studies have shown that the presence (and chemical composition) of the oxide layer above the 2D material can have a significant effect on the outcome of the SPL process, and could be one contributing factor to the differing outcomes.

2.2. Other Subtractive SPL Methods

Other subtractive-SPL methods have also been applied for the lithography of 2D materials in a number of reports, including thermochemical-SPL (tc-SPL),[81–83] and mechanical-SPL (m-SPL).[84–87]

2.2.1. Thermochemical-SPL

In broad terms, tc-SPL employs a heated probe to initiate a local thermally driven reaction. The first reported example[81] employed tc-SPL on a GO sheet to generate rGO lines with an FWHM of ≈25 nm. Using a heated probe under an inert (nitrogen) atmosphere at a v_{tip} of 2000 nm s^{-1}, different regions were pattered in the form of squares at different temperatures in the range of 100–700 °C. An analysis postlithography with lateral force microscopy showed that regions patterned at higher temperatures showed lower friction (−12 nN at 700 °C vs −1 nN at 130 °C). These results were supported by sheet resistance measurements in the SPL-generated features (at 1200 °C) that gave values that were comparable to rGO films produced by overnight thermal annealing at 600 °C (18 kΩ) compared to the unmodified GO film (427 MΩ).

Luo and Wang et al.[82] on the other hand, demonstrated the generation of rGO patterns on SLGO at a lower temperature (≤115 °C) using a Pt-coated AFM tip in the presence of H_2 gas. Here, the Pt-coated AFM tip acted as a catalyst for the reduction of GO, thus avoiding the need for the higher temperatures reported above. Best results were achieved at 100 °C and a v_{tip} of 1 nm s^{-1}, which led to the generation of 2 µm long rGO lines with an FWHM of ≈80 nm. The conductivity of this linear feature was determined to be ≈10^3 S m^{-1}, within the same order of magnitude as that for chemically generated rGO.[88] The fact that this method relied on a catalytic reduction reaction was confirmed with control experiments, where the use of uncoated probes or in vacuum did not give rise to any features.

Based on these reports, it can be concluded that tc-SPL of graphene oxide leads to the formation of nanoscale features with properties that are consistent with rGO. The use of Pt as a catalyst to enable reductions under milder conditions is notable and a good example of "catalytic SPL,[30]" which is an emerging area of SPL research.

2.2.2. Mechanical-SPL

m-SPL perhaps represents the most rudimentary method of SPL, wherein the direct application of force by the probe induces removal of material from a surface (cf. "nanoscratching"). The first example of this approach as applied to 2D materials was by Zhang and co-workers,[84] on BLGO using a Si tip with various set points (SPs) in the range of 1 to 5 V. Complete removal of the GO film, resulting in a GO-free gap, was obtained at SP of 3 V. Whereas, smaller forces (equivalent to an SP of 1 V) did not lead to complete scratching of GO. By controlling the spacing between the parallel scratched lines, GO "nanoribbons" with varying widths from 56 to 110 nm were achieved. However, it is not possible to draw any relationships between the line width and the force applied, since the relationship between SP and force was not given in this report. Furthermore, the SP used for the particular feature widths was also not provided.

Besides generating nanoscale features of GO, m-SPL has also been used to fabricate structures for the study of charge transport along the SiO_2 surface between isolated and grounded graphene sheets (**Figure 8**a).[86] In this experiment, a diamond-coated AFM tip was scanned at a high load force (1000 nN) to cut a graphene sheet into separate isolated and grounded sections (Figure 8a–c) with gap widths from 40 to 2000 nm. However, the authors did not give any details of the experiment and how they achieved different gap widths between two graphene sheets.

Overall, subtractive SPL methods represent some of the earliest SPL methods, as their equipment set up and operation are relatively straightforward. Their applicability has been demonstrated on a wide range of 2D materials, including in the fabrication of working devices. The sizes of the features generated can be tailored by varying V_{tip}, v_{tip}, and RH in the case of electrochemical SPL methods; probe temperature for tc-SPL; and

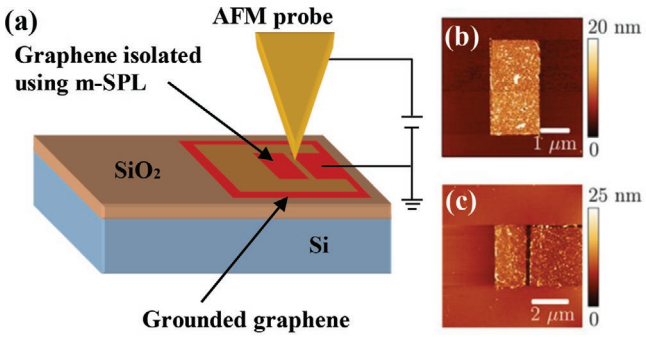

Figure 8. a) Schematic diagram illustrating SPL setup used to study the charge transport. AFM topography image of b) the single rectangular isolated graphene sheet, and c) an isolated graphene sheet separated by the gap from grounded graphene. (b,c) Reproduced with permission.[86] Copyright 2018, American Chemical Society.

contact force in m-SPL. A major advantage for tc- and m-SPL in comparison to electrochemical SPL is that they are not limited by the type of substrate material. Electrochemical-SPL using DC bias is constrained by the need for a conductive substrate to enable electron flow that drives the redox reactions, though electrochemical-SPL with an AC bias could be used for nonconducting substrates, thus offering a route for the application of electrochemical-SPL for wider range of materials. In terms of its disadvantages, tc-SPL is performed as high temperatures (>100 °C), which obviously means that it cannot be used for heat sensitive applications. In m-SPL, the limiting factor in creating reproducible patterns is the stability of the tip, which is prone to deformation, breakage and contamination from the debris of the scratched material.

3. Additive ("Constructive") Nanolithography on 2D Materials

3.1. Dip-Pen Nanolithography (DPN)

As noted above, DPN utilizes a water meniscus that forms at the point of contact between tip and surface to enable the capillary transport of small molecules (Figure 1b). Thus, molecular transport in DPN depends on RH, v_{tip} (or dwell time), temperature, and the physicochemical properties of both the ink and the surface.

As a first example of its application to 2D materials, DPN has been used to deposit Co nanoparticles on SLG, while preserving the properties of SLG.[89] The ink formulation in this case consisted of a colloid of oleic acid-stabilized Co nanoparticles (≈7.6 nm) in *o*-dichlorobenzene. In order to coat the probe with the nanoparticles, this ink was deposited on to a SiO_2 surface, left to partially evaporate and the probe tip scanned across the droplet. This "inked" probe was then used to perform lithography at an RH of 50%, and gave spot features ≈675 nm in diameter on SLG. However, the contact time of the probe on the spots during lithography was not reported. Nevertheless, Raman spectroscopy and electronic transport measurements suggests that graphene's structure and conductivity were not altered after the deposition of the nanoparticles. This result therefore demonstrates that DPN enables the deposition of nanoparticles under mild ambient conditions that do not damage the underlying 2D material, which is difficult to achieve through conventional "hard" lithographic methods.

Mirkin and co-workers[90] employed DPN on SLG where line features were produced by the writing of rhodamine 6G (R6G), a fluorescent dye. In common with previous DPN experiments on non-2D materials, the treatment of the probes with O_2 plasma was necessary to render them hydrophilic, in order to facilitate molecular transport. When the appropriate amount of dye was present on the probes, it was found that the FWHM of the patterned line features was negatively correlated with the v_{tip}; with line FWHM of ≈90, 130, and 180 nm being produced at v_{tip} of 100, 50, and 20 nm s^{-1}, respectively, at an RH of 75%. Further, lines with an FWHM as small as 45 nm could be produced, though the v_{tip} was not reported. It was also found that the concentration of the R6G solution that was coated on the probes prior to the lithography also had an effect on the feature height. High concentrations (1000×10^{-6} M) resulted in heights of ≈1 nm (estimated to be the thickness of two dye molecules), while dilute solutions (10×10^{-6} M) gave features with a height of ≈0.4 nm (approximately one dye molecule). However, the pattern fidelity, stability upon storage and reproducibility or the dye monolayer features produced from these lower concentrations of ink were generally poor, suggesting that the dye molecules deposited as monolayers were somewhat mobile on the surface.

The authors then subsequently studied the electronic properties of graphene patterned with the bilayer features by Kelvin probe force microscopy and found that the lines exhibited a contact potential reduction of 22 mV between the surface and the probe, which indicated n-type doping of the patterned areas compared to pristine graphene. These results thus demonstrate how the deposition of small molecules on graphene by DPN can be used to engineer its electronic properties.

In another report, DPN has also been used to demonstrate the deposition of phospholipids on SLG.[91] Here, DPN was used to write mixtures of the lipid 1,2-dioleoyl-sn-glycero-3-phosphocholine (DOPC) with DOPC derivatives that were labeled with the fluorescent dye lissamine rhodamine or the biological cofactor biotin. It was previously known that such lipid mixtures could be deposited by DPN on to hydrophilic substrates such as SiO_2.[92] However, when using the same conditions that gave well-defined features on SiO_2, it was found that only large and poorly defined patches of lipids were deposited on to the graphene. AFM imaging of these patches revealed that the phospholipids diffused and assembled into monolayers on the graphene, which the authors proposed was due to the higher mobility of the phospholipids on the hydrophobic graphene surface. The effect of this spreading on feature size was then investigated and it was found to be dependent on the humidity of the environment. As expected, larger widths with increasing RH and decreasing v_{tip} were observed, and are consistent with the diffusion of thiols that had been written on gold by DPN.[93] Subsequently, this report demonstrated the feasibility of using the physisorbed lipid patches on graphene for the selective binding of a protein. Here, the biotin-functionalized lipids were able to capture a fluorescently labeled streptavidin, which can then be observed by fluorescence microscopy.

In a follow-on study, the feasibility of using multipen DPN to functionalize isolated 1×1 μm^2 graphene patches with different lipid mixtures in a single parallelized write cycle was performed by the same group.[94] In this case a linear series of cantilevers (a so-called "1D" array), each coated with different lipid mixtures was used. Due to the high mobility of the lipids, simply by bringing the probes into contact with each patch (at 40% RH) it was found that the lipids diffused from the probe to cover the entire patch in ≈10 s. Notably, the spread of the lipids was self-limited to the graphene patches and did not diffuse further on to the SiO_2 substrates. The use of multipen DPN here is significant, as it represents an example of how parallelized SPL can be used for fabrication over large areas.

In terms of device fabrication, Bao and co-workers[95] have described the use of DPN to template the etching of SLG and the subsequent of deposition of metal contacts. To demonstrate the procedure, a Au film was first thermally deposited over exfoliated SLG flakes and DPN was then used to write

16-mercaptohexadecanoic acid (MHA) features on to the film. Here MHA acts as an etch resist, such that subsequent wet etching resulted in the MHA-masked Au remaining only in the areas defined by DPN. The pattern can then be transferred to the underlying SLG as the Au film in turn acted as a resist against O_2 plasma etching. Using this procedure, SLG features of sizes as small as 1 μm could be produced. Subsequently, the Au electrical contacts could be defined on the etched SLG through a similar process of Au film deposition, DPN of the MHA and wet etching of the bulk unpatterned Au. The SLG flake fabricated and wired in this manner gave a sheet resistance of ≈4.6 kΩ, which was comparable to reported values (≈6.5 kΩ) of SLG-based devices fabricated by standard methods that included EBL.[2] This result therefore suggests that DPN may offer a low-cost approach for SLG fabrication.

Shin et al.[96] have described the use of DPN to deposit polystyrene (PS) as a resist material for the fabrication of graphene nanoribbon (GNR)-based FETs on a $SrTiO_3$/Nb-doped $SrTiO_3$ substrate. Using a solution of polystyrene in toluene as the ink and a v_{tip} from 50 to 300 nm s^{-1}, rod-shaped features with widths of 150 to 30 nm were written on SLG sheets. These PS features thus acted as a resist for the subsequent O_2 plasma treatment, and could afterward be removed by dissolution in organic solvents to leave the underlying (unetched) GNRs. In order to fabricate the FET source and drain contacts, DPN was then used to deposit a $PbCl_2$ solution at each end of the GNR, which upon thermal annealing produced a Pb dot feature. These Pb dots were then wired to the external circuit by Au wires, which were produced by the thermal annealing of $AuCl_4$ lines that was also written by DPN.

Characterization of an FET fabricated in this way (based on a GNR 150 × 50 nm^2 in size and using the Nb-doped substrate as the gate) demonstrated bipolar FET behavior with a high electron mobility (3150 cm^2 V^{-1} s^{-1} at 300 K) and a low operating voltage ($V_g \approx 0.1$ V), which was attributed to the flat surface and large dielectric constant of the insulating $SrTiO_3$ layer, respectively. However, this report fails to disclose many of the experimental details for the DPN (including the RH, molecular weight, and concentration of the PS), which makes it difficult to draw any meaningful insights into general applicability of this procedure.

Nonetheless, these latter two reports are noteworthy as examples where all the lithography steps (both for the transistor material and the connections) were performed by DPN alone, thus circumventing the need for any steps that involved conventional "hard" lithographic methods.

3.2. Polymer Pen Lithography (PPL)

PPL represents a method that combines the advantages of multiprobe DPN with the ease of use, cost and robustness of microcontact printing. Due to the deformability of the probes, an added facet of PPL is that the properties of the printed feature can also be manipulated through the amount of force exerted by the probes. Braunschweig and co-workers have explored the possibility of using PPL to print and covalently attach functionalized cyclopentadienes on to SLG using the Diels-Alder reaction.[97] Here, PPL experiments were performed using a dye-functionalized cyclopentadiene that was printed with a force of 100 mN for 30 min, leading to the formation of dot features with a diameter of 10 μm. An analysis of these features by Raman spectroscopy showed spectral changes to the SLG, which authors proposed were the result of a force-induced Diels–Alder reaction between the cyclopentadiene group and the SLG, consistent with previous observations for Diels–Alder reactions on SLG surfaces.[98]

In order to determine if the printed cyclopentadienes were able to electronically interact with the SLG, ferrocene-functionalized molecules were printed. These surfaces were then analyzed by cyclic voltammetry using the patterned SLG as an electrode and showed a strong redox peak at E_o = 590 mV (vs Ag/AgCl) confirming the presence of a ferrocene/ferrocenium reversible redox couple on the surface. These results therefore showed that electronic coupling was indeed achieved.

Overall, this report is interesting as it demonstrates how PPL can be used not only for the deposition of a molecular ink in a parallelized manner over large areas, but also to drive a chemical reaction through the application of force. It thus represents an example of a mechanochemical reaction applied to SPL.

4. Conclusions and Future Perspectives

Graphene and other 2D materials are currently being studied extensively due to their unique physicochemical properties, which are promising for a wide range of applications. In terms of the fabrication of miniaturized devices, there remains a fundamental need for (nano)lithography tools that are more convenient in comparison to classical cleanroom-based "hard" methods, in terms of flexibility, energy, and capital intensiveness. In this regard, SPL as an alternative lithographic approach has drawn considerable attention, and a range of subtractive and additive SPL techniques have been reported that operate through a variety of chemical and physical phenomena to modify 2D materials.

A survey of the literature to date shows that electrochemical SPL methods have been the most widely applied to 2D materials, and both oxidation and reduction reactions have been demonstrated. In the case of graphene, the ability to produce graphene with a range of oxidized or reduced states is extremely useful because it enables the fabrication of devices with a range of electronic properties, and in some cases with properties that cannot be achieved through conventional processing methods.

The versatility of additive molecular printing tools such as DPN and PPL makes them particularly interesting as they enable the deposition of "soft" materials such as complex organic molecules and polymers, which would be useful for the fabrication of devices intended for biomedical use (e.g., biosensors and diagnostics). Significantly, DPN has not only been shown to enable the lithography of 2D materials, but also the metal electrodes needed to wire them to an external circuit. Combined with the fact that it can be carried out in a multiplexed manner, DPN (and PPL) thus offer the possibility of solely using SPL for the large-scale fabrication of devices. Indeed, since nearly all of the SPL methods reported so far are serial in nature, such demonstrations of high-throughput lithography represent an important step toward practical applications

in manufacturing. Indeed, large arrays of scanning probes for DPN containing up to 55000 probes over a 1 cm^2 area[99] and PPL probe arrays consisting of up to 11 million probes over 182 cm^2 (on a 3″ wafer)[34] are documented, and represent a clear route toward scale-up.

The main limitation currently in this field is that all the above studies represent "proof-of-concept" examples that mainly aim to demonstrate feasibility. In many cases full and unambiguous experimental details have not been given, making it difficult to systematically correlate the observed results with the various SPL parameters used, and impossible to reproduce independently. A related issue is the fact that many of the 2D materials used are poorly characterized (or their detailed characteristics not reported), and as a result what are superficially the same lithography conditions give very different outcomes (e.g., in the case of MoS_2). Examples of characteristics that are almost never analyzed or reported, but which could affect the lithography, include the presence of impurities in the substrate, the presence of adsorbed materials, the nature of the overlying oxide layer, the crystal domain size, and the quantity and nature of any defects. Furthermore, there remains a lack of systematic studies aimed at gaining insights into physicochemical mechanisms of feature formation. Addressing the characterization and knowledge gap will be crucial toward the development of practical SPL methods.

The field of SPL encompasses a great variety of very different experimental methodologies and concepts, resulting in an equally wide range of outcomes. Combined with the fact that technical details are often incompletely described, this means that comparative analyses between the different types of SPL (and even between individual reports using the same technique) are difficult. Further research in this area would therefore benefit from the development of a set of community/industry standards and figures of merit, against which these SPL methods can be compared.

One possible future direction in the further development of SPL for 2D materials is the implementation of more advanced "chemical" methods.[100] For example, the application of scanning probes bearing catalysts (including organocatalysts and biocatalysts)[30,31,101] that are able to direct specific chemical reactions for the synthesis of more complex structures. Harnessing probes that are able to perform near-field optical lithography[102,103] to direct photochemical reactions are also a possibility. In practical terms, improvements in the user-friendliness of SPL equipment would also facilitate the uptake of this technology. For example, the development of automation for multiplexed SPL.[104,105]

The high level of interest in 2D materials means that there is likely to be continuing demand for methods that are accessible to nonspecialists in lithography and enable the implementation of arbitrary device designs for rapid prototyping. SPL-based methods and equipment are therefore uniquely suitable for the fast, flexible, and convenient "desk-top fabrication[106]" of 2D materials.

Acknowledgements

The authors thank the British Council Newton Fund for support under Contract No. 216196834 and the UK Engineering and Physical Sciences Research Council under Grant Nos. EP/K024485/1 and EP/K011685/1. The authors also thank Laura Weatherburn for assistance in the preparation of the manuscript.

Conflict of Interest

The authors declare no conflict of interest.

Keywords

2D materials, additive lithography, graphene, scanning probe nanolithography, subtractive lithography

Received: February 27, 2019
Revised: April 3, 2019
Published online: June 13, 2019

[1] K. S. Novoselov, A. K. Geim, S. V. Morozov, D. Jiang, Y. Zhang, S. V. Dubonos, I. V. Grigorieva, A. A. Firsov, *Science* **2004**, *306*, 666.
[2] K. S. Novoselov, A. K. Geim, S. V. Morozov, D. Jiang, M. Katsnelson, I. Grigorieva, S. V. Dubonos, A. Firsov, *Nature* **2005**, *438*, 197.
[3] R. Mas-Balleste, C. Gomez-Navarro, J. Gomez-Herrero, F. Zamora, *Nanoscale* **2011**, *3*, 20.
[4] J. Ahn, B. H. Hong, *Nat. Nanotechnol.* **2014**, *9*, 737.
[5] D. Akinwande, N. Petrone, J. Hone, *Nat. Commun.* **2014**, *5*, 5678.
[6] H. Liu, A. T. Neal, Z. Zhu, Z. Luo, X. Xu, D. Tomanek, P. D. Ye, *ACS Nano* **2014**, *8*, 4033.
[7] R. Ganatra, Q. Zhang, *ACS Nano* **2014**, *8*, 4074.
[8] M. J. Allen, V. C. Tung, R. B. Kaner, *Chem. Rev.* **2010**, *110*, 132.
[9] Y. Zhang, Y.-W. Tan, H. L. Stormer, P. Kim, *Nature* **2005**, *438*, 201.
[10] B. Radisavljevic, A. Radenovic, J. Brivio, V. Giacometti, A. Kis, *Nat. Nanotechnol.* **2011**, *6*, 147.
[11] H. Fang, M. Tosun, G. Seol, T. C. Chang, K. Takei, A. Javey, *Nano Lett.* **2013**, *13*, 1991.
[12] D. Chimene, D. L. Alge, A. K. Gaharwar, *Adv. Mater.* **2015**, *27*, 7261.
[13] Y. Zheng, H. Wang, S. Hou, D. Xia, *Adv. Mater. Technol.* **2017**, *2*, 1600237.
[14] J. Fan, J. M. Michalik, L. Casado, S. Roddaro, M. R. Ibarra, J. M. De Teresa, *Solid State Commun.* **2011**, *151*, 1574.
[15] L. Li, Y. Yu, G. J. Ye, Q. Ge, X. Ou, H. Wu, D. Feng, X. Hui Chen, Y. Zhang, *Nat. Nanotechnol.* **2014**, *9*, 372.
[16] W. Xu, T. Lee, *Mater. Horiz.* **2016**, *3*, 186.
[17] H. Kwon, P. J. Jeon, J. S. Kim, T. Kim, H. Yun, S. W. Lee, T. Lee, S. Im, *2D Mater.* **2016**, *3*, 044001.
[18] P. Han, L. St. Marie, Q. X Wang, N. Quirk, A. El Fatimy, M. Ishigami, P. Barbara, *Nanotechnology* **2018**, *29*, 20LT01.
[19] K. Yamazaki, A. Fujiwara, Y. Takahashi, H. Namatsu, K. Kurihara, *Jpn. J. Appl. Phys.* **1998**, *37*, 44.
[20] S. Fujii, T. Enoki, *Acc. Chem. Res.* **2013**, *46*, 2202.
[21] M. Tinoco, L. Maduro, M. Masaki, E. Okunishi, S. Conesa-Boj, *Nano Lett.* **2017**, *17*, 7021.
[22] X. Peng, A. Copple, Q. Wei, *J. Appl. Phys.* **2014**, *116*, 144301.
[23] A. N. Abbas, G. Liu, B. Liu, L. Zhang, H. Liu, D. Ohlberg, W. Wu, C. Zhou, *ACS Nano* **2014**, *8*, 1538.
[24] Y. Zhang, C. Hui, R. Sun, K. Li, K. He, X. Ma, F. Liu, *Nanotechnology* **2014**, *25*, 135301.
[25] R. D. Piner, J. Zhu, F. Xu, S. Hong, C. A. Mirkin, *Science* **1999**, *283*, 661.
[26] K. Salaita, Y. Wang, C. A. Mirkin, *Nat. Nanotechnol.* **2007**, *2*, 145.
[27] R. Garcia, A. W. Knoll, E. Riedo, *Nat. Nanotechnol.* **2014**, *9*, 577.
[28] R. Garcia, R. V. Martinez, J. Martinez, *Chem. Soc. Rev.* **2006**, *35*, 29.
[29] C. R. Kinser, M. J. Schmitz, M. C. Hersam, *Nano Lett.* **2005**, *5*, 91.
[30] S. A. M. Carnally, L. S. Wong, *Nanoscale* **2014**, *6*, 4998.
[31] J. Hosford, M. Valles, F. W. Krainer, A. Glieder, L. S. Wong, *Nanoscale* **2018**, *10*, 7185.

[32] H. Mamin, D. Rugar, *Appl. Phys. Lett.* **1992**, *61*, 1003.
[33] A. A. Tseng, *Small* **2011**, *7*, 3409.
[34] F. Huo, Z. Zheng, G. Zheng, L. R. Giam, H. Zhang, C. A. Mirkin, *Science* **2008**, *321*, 1658.
[35] C. A. Mirkin, *ACS Nano* **2007**, *1*, 79.
[36] Y. K. Ryu, R. Garcia, *Nanotechnology* **2017**, *28*, 142003.
[37] N. Kurra, R. G. Reifenberger, G. U. Kulkarni, *ACS Appl. Mater. Interfaces* **2014**, *6*, 6147.
[38] A. J. M. Giesbers, U. Zeitler, S. Neubeck, F. Freitag, K. S. Novoselov, J. C. Maan, *Solid State Commun.* **2008**, *147*, 366.
[39] L. Weng, L. Zhang, Y. P. Chen, L. P. Rokhinson, *Appl. Phys. Lett.* **2008**, *93*, 093107.
[40] S. Masubuchi, M. Ono, K. Yoshida, K. Hirakawa, T. Machida, *Appl. Phys. Lett.* **2009**, *94*, 082107.
[41] S. Neubeck, F. Freitag, R. Yang, K. S. Novoselov, *Phys. Status Solidi B* **2010**, *247*, 2904.
[42] S. Masubuchi, M. Arai, T. Machida, *Nano Lett.* **2011**, *11*, 4542.
[43] R. K. Puddy, P. H. Scard, D. Tyndall, M. R. Connolly, C. G. Smith, G. A. C. Jones, A. Lombardo, A. C. Ferrari, M. R. Buitelaar, *Appl. Phys. Lett.* **2011**, *98*, 133120.
[44] I. Byun, D. Yoon, J. S. Choi, I. Hwang, D. H. Lee, M. J. Lee, T. Kawai, Y. Son, Q. Jia, H. Cheong, B. H. Park, *ACS Nano* **2011**, *5*, 6417.
[45] H. Yong, K. Kim, W. Choi, J. Park, M. Ahmad, Y. Seo, *Carbon* **2012**, *50*, 4640.
[46] M. Chuang, H. Chien, Y. Chain, G. Chi, S. Lee, W. Y. Woon, *Carbon* **2013**, *54*, 336.
[47] R. K. Puddy, C. J. Chua, M. R. Buitelaar, *Appl. Phys. Lett.* **2013**, *103*, 183117.
[48] M. Ahmad, Y. Seo, Y. J. Choi, *Micro Nano Lett.* **2013**, *8*, 422.
[49] T. Gowthami, M. Gadhewal, G. Raina, *IEEE Trans. Nanotechnol.* **2013**, *12*, 1002.
[50] I. Byun, W. Kim, D. W. Boukhvalov, I. Hwang, J. W. Son, G. Oh, J. S. Choi, D. Yoon, H. Cheong, J. Baik, H. Shin, H. W. Shiu, C. Chen, Y. Son, B. H. Park, *NPG Asia Mater.* **2014**, *6*, e102.
[51] H. Chien, M. Chuang, H. Tsai, H. Shiu, L. Chang, C. Chen, S. Lee, J. White, W. Woon, *Carbon* **2014**, *80*, 318.
[52] M. Arai, S. Masubuchi, K. Nose, Y. Mitsuda, T. Machida, *Jpn. J. Appl. Phys.* **2015**, *54*, 04DJ06.
[53] D. H. Lee, C. K. Kim, J. Lee, H. Chung, B. H. Park, *Carbon* **2016**, *96*, 223.
[54] S. A. G. Barragan, S. Zimmermann, S. Fatikow, *IEEE Nanotechnology Material and Devices (NMDC)*, IEEE, Singapore **2017**, pp. 49–50.
[55] A. I. Dago, S. Sangiao, R. Fernandez-Pacheco, J. M. De Teresa, R. Garcia, *Carbon* **2018**, *129*, 281.
[56] G. Rius, N. Camara, P. Godignon, F. Pérez-Murano, N. Mestres, *J. Vac. Sci. Technol., B: Microelectron. Nanometer Struct.–Process., Meas., Phenom.* **2009**, *27*, 3149.
[57] J. M. P. Alaboson, Q. H. Wang, J. A. Kellar, J. Park, J. W. Elam, M. J. Pellin, M. C. Hersam, *Adv. Mater.* **2011**, *23*, 2181.
[58] F. Colangelo, V. Piazza, C. Coletti, S. Roddaro, F. Beltram, P. Pingue, *Nanotechnology* **2017**, *28*, 105709.
[59] Y. Hong, W. Chiang, H. Tsai, M. Chuang, Y. Kuo, L. Chang, C. Chen, J. White, W. Woon, *Nanotechnology* **2017**, *28*, 395704.
[60] Y. Wang, Y. Hong, L. Chang, C. Chen, W. Woon, *J. Phys. Chem. C* **2018**, *122*, 15786.
[61] A. San Paulo, R. García, *Phys. Rev. B* **2001**, *64*, 193411.
[62] J. A. Dagata, J. Schneir, H. H. Harary, C. J. Evans, M. T. Postek, J. Bennett, *Appl. Phys. Lett.* **2001**, *56*, 1990.
[63] D. Yang, A. Velamakanni, G. Bozoklu, S. Park, R. D. Piner, S. Stankovich, I. Jung, D. A. Field, J. C. A. Ventrice, R. S. Ruoff, *Carbon* **2009**, *47*, 145.
[64] S. Stankovich, R. D. Piner, X. Q. Chen, N. Q. Wu, S. T. Nguyen, R. S. Ruoff, *J. Mater. Chem.* **2006**, *16*, 155.
[65] Z. Luo, T. Yu, K.-J. Kim, Z. Ni, Y. You, S. Lim, Z. Shen, S. Wang, J. Lin, *ACS Nano* **2009**, *3*, 1781.
[66] J. M. Mativetsky, E. Treossi, E. Orgiu, M. Melucci, G. P. Veronese, P. Samorı, V. Palermo, *J. Am. Chem. Soc.* **2010**, *132*, 14130.
[67] A. C. Faucett, J. M. Mativetsky, *Carbon* **2015**, *95*, 1069.
[68] M. Lorenzoni, A. Giugni, E. Di Fabrizio, F. Pérez-Murano, A. Mescola, B. Torre, *Nanotechnology* **2015**, *26*, 285301.
[69] E. Climent-Pascual, M. Garcıa-Velez, A. L. Alvarez, C. Coya, C. Munuera, X. Dıez-Betriu, M. Garcıa-Hernandez, A. de Andres, *Carbon* **2015**, *90*, 110.
[70] F. Schwierz, *Nat. Nanotechnol.* **2010**, *5*, 487.
[71] G. Jnawali, H. Lee, J. Lee, M. Huang, J. Hsu, F. Bi, R. Zhou, G. Cheng, B. D'Urso, P. Irvin, C. Eom, J. Levy, *ACS Nano* **2018**, *12*, 6128.
[72] S. Thiel, G. Hammerl, A. Schmehl, C. W. Schneider, J. Mannhart, *Science* **2006**, *313*, 1942.
[73] X. Liu, K. Chen, S. A. Wells, I. Balla, J. Zhu, J. D. Wood, M. C. Hersam, *Adv. Mater.* **2017**, *29*, 1604121.
[74] P. Yasaei, B. Kumar, T. Foroozan, C. Wang, M. Asadi, D. Tuschel, J. E. Indacochea, R. F. Klie, A. Salehi-Khojin, *Adv. Mater.* **2015**, *27*, 1887.
[75] J. Kang, J. D. Wood, S. A. Wells, J.-H. Lee, X. Liu, K.-S. Chen, M. C. Hersam, *ACS Nano* **2015**, *9*, 3596.
[76] T. F. D. Fernandes, A. de C. Gadelha, A. P. M. Barboza, R. M. Paniago, L. C. Campos, P. S. S. Guimarães, P. de Assis, B. R. A. Neves, *2D Mater.* **2018**, *5*, 025018.
[77] M. Donarelli, F. Perrozzi, F. Bisti, F. Paparella, V. Feyer, A. Ponzoni, M. Gonchigsuren, L. Ottaviano, *Nanoscale* **2015**, *7*, 11453.
[78] F. M. Espinosa, Y. K. Ryu, K. Marinov, D. Dumcenco, A. Kis, R. Garcia, *Appl. Phys. Lett.* **2015**, *106*, 103503.
[79] A. I. Dago, Y. K. Ryu, R. Garcia, *Appl. Phys. Lett.* **2016**, *109*, 163103.
[80] A. I. Dago, Y. K. Ryu, F. J. Palomares, R. Garcia, *ACS Appl. Mater. Interfaces* **2018**, *10*, 40054.
[81] Z. Wei, D. Wang, S. Kim, S. Kim, Y. Hu, M. K. Yakes, A. R. Laracuente, Z. Dai, S. R. Marder, C. Berger, W. P. King, W. A. de Heer, P. E. Sheehan, E. Riedo, *Science* **2010**, *328*, 1373.
[82] K. Zhang, Q. Fu, N. Pan, X. Yu, J. Liu, Y. Luo, X. Wang, J. Yang, J. Hou, *Nat. Commun.* **2012**, *3*, 1194.
[83] Y. Choi, X. Wu, D. Lee, *Rev. Sci. Instrum.* **2014**, *85*, 045002.
[84] G. Lu, X. Zhou, H. Li, Z. Yin, B. Li, L. Huang, F. Boey, H. Zhang, *Langmuir* **2010**, *26*, 6164.
[85] Y. He, H. Dong, T. Li, C. Wang, W. Shao, Y. Zhang, L. Jiang, W. Hu, *Appl. Phys. Lett.* **2010**, *97*, 133301.
[86] M. Konečný, M. Bartošík, J. Mach, V. Švarc, D. Nezval, J. Piastek, P. Procházka, A. Cahlík, T. Šikola, *ACS Appl. Mater. Interfaces* **2018**, *10*, 11987.
[87] X. Tang, K. W. C. Lai, *IEEE Trans. Nanotechnol.* **2016**, *15*, 607.
[88] Y. C. Si, E. T. Samulski, *Nano Lett.* **2008**, *8*, 1679.
[89] E. Bellido, I. O. Jiménez, A. Ghirri, C. Alvino, A. Candini, V. Puntes, M. Affronte, N. Domingo, D. Ruiz-Molina, *Langmuir* **2012**, *28*, 12400.
[90] X. Zhou, S. He, K. A. Brown, J. Mendez-Arroyo, F. Boey, C. A. Mirkin, *Nano Lett.* **2013**, *13*, 1616.
[91] M. Hirtz, A. Oikonomou, T. Georgiou, H. Fuchs, A. Vijayaraghavan, *Nat. Commun.* **2013**, *4*, 2591.
[92] S. Lenhert, P. Sun, Y. Wang, H. Fuchs, C. A. Mirkin, *Small* **2007**, *3*, 71.
[93] K. A. Brown, D. J. Eichelsdoerfer, X. Liao, S. He, C. A. Mirkin, *Front. Phys.* **2014**, *9*, 385.
[94] M. Hirtz, A. Oikonomou, N. Clark, Y. Kim, H. Fuchs, A. Vijayaraghavan, *Nanoscale* **2016**, *8*, 15147.
[95] W. M. Wang, N. Stander, R. M. Stoltenberg, D. Goldhaber-Gordon, Z. Bao, *ACS Nano* **2010**, *4*, 6409.
[96] Y. Shin, J. Y. Son, M. Jo, Y. Shin, H. M. Jang, *J. Am. Chem. Soc.* **2011**, *133*, 5623.
[97] S. Bian, A. M. Scott, Y. Cao, Y. Liang, S. Osuna, K. N. Houk, A. B. Braunschweig, *J. Am. Chem. Soc.* **2013**, *135*, 9240.

[98] S. Sarkar, E. Bekyarova, S. Niyogi, R. C. Haddon, *J. Am. Chem. Soc.* **2011**, *133*, 3324.
[99] K. Salaita, Y. Wang, J. Fragala, R. A. Vega, C. Liu, C. A. Mirkin, *Angew. Chem., Int. Ed.* **2006**, *45*, 7220.
[100] S. Clair, D. G. de Oteyza, *Chem. Rev.* **2019**, *119*, 4717.
[101] J. Botton, K. Gratzer, C. Francois, V. Mesquita, L. Patrone, T. S. Balaban, S. Clair, J. Parrain, O. Chuzel, *Chem. Sci.* **2018**, *9*, 4280.
[102] F. Huo, G. Zheng, X. Liao, L. R. Giam, J. Chai, X. Chen, W. Shim, C. A. Mirkin, *Nat. Nanotechnol.* **2010**, *5*, 637.
[103] E. ul-Haq, Z. Liu, Y. Zhang, S. A. A. Ahmad, L. S. Wong, J. K. Hobbs, G. J. Leggett, J. Micklefield, C. J. Roberts, J. M. R. Weaver, *J. Mater. Res.* **2011**, *26*, 2997.
[104] S. Wang, J. Hosford, W. P. Heath, L. S. Wong, *RSC Adv.* **2015**, *5*, 61402.
[105] I. Lee, J. Hosford, S. Wang, J. A. Hunt, J. M. Curran, W. P. Heath, L. S. Wong, *J. Vis. Exp.* **2018**, *136*, e56967.
[106] L. R. Giam, A. J. Senesi, X. Liao, L. S. Wong, J. Chai, D. J. Eichelsdoerfer, W. Shim, B. Rasin, S. He, C. A. Mirkin, *Proc. SPIE* **2011**, *8031*, 803103.